Theoretical Derivation of Aerosol Lidar Ratio using Mie Theory for CALIOP-CALIPSO and OPAC Aerosol Models

Radhika A. Chipade[1] and Mehul R. Pandya[1]

[1]Space Applications Centre (ISRO), Ahmedabad, Gujarat, India – 380015.

Correspondence to: Radhika A. Chipade (radhikachipade@gmail.com)

Abstract. The extinction-to-backscattering ratio, popularly known as lidar (light detection and ranging) ratio of atmospheric aerosols is an important optical property, which is essential to retrieve the extinction profiles of atmospheric aerosols. Lidar satellite observations can provide the global coverage of atmospheric aerosols along with their vertical extent. NASA's Cloud-Aerosol Lidar with Orthogonal Polarisation (CALIOP) on-board Cloud-Aerosol Lidar and Infrared Pathfinder Satellite Observations (CALIPSO) is the only space-based platform available so far, that provides the vertical profiles of extinction due to atmospheric aerosols. A physics-based theoretical approach is presented in the present paper that estimates lidar ratio values for CALIPSO aerosol models, which can be used as inputs to determine the extinction profiles of aerosols using CALIPSO data. The developed methodology was also qualified by comparing it with the lidar ratio values derived using AERONET datasets. Lidar ratio for CALIPSO aerosols models were estimated in the range of 38.72 sr to 85.98 sr at 532 nm whereas, at 1064 nm lidar ratio varied between 20.11 sr to 71.11 sr depending upon the aerosol type and their size distributions.

Aerosols are compositions of various particles and thus the presence of water vapour in the atmosphere can affect the optical properties of the aerosols. Thus, the effect of relative humidity on lidar ratio was studied using Optical Properties of Cloud and Aerosols software tool (OPAC) aerosol models, which are the standard aerosol models against the cluster classified AERONET and CALIPSO aerosol models. Water soluble particles contribute substantially in clean continental, clean marine, tropical marine and desert aerosol models and are hygroscopic in nature. Hygroscopic sulfate particles dominate the Antarctic aerosols during summertime. In presence of relative humidity between 0 – 80%, the lidar ratio values were observed to decrease from 53.59 sr to 47.13 sr, 53.66 sr to 47.15 sr, 53.70 sr to 47.16 sr and 55.32 sr to 48.78 sr at 532 nm for clean continental, clean marine, tropical marine and desert aerosols, respectively, whereas lidar ratio gradually increased from 47.13 sr to 51 sr, 47.15 sr to 51 sr, 47.16 sr to 51 sr and 48.78 sr to 51.68 sr, respectively for these aerosol models when relative humidity was between 80 – 99%; due to constituent hygroscopic particles. In case of Antarctic aerosols, the lidar ratio was observed to increase from 57.73 sr to 97.64 sr due to hygroscopic sulfate particles that backscattered heavily in presence of water vapour at 532 nm. The soot particles dominate the polluted continental and polluted marine particles causing an increase in lidar ratio over corresponding clean counterpart. Similar results were observed at 1064 nm for OPAC aerosol models.

1 Introduction:

The light detection and ranging (lidar) measurements are considered appropriate to retrieve the range-resolved values of vertical backscatter and extinction profiles of tropospheric aerosols. The single scattering lidar equation is solved in order to determine extinction and backscatter profiles of aerosols, which depends on the ratio of

extinction-to-backscatter coefficient, known as lidar ratio. Thus, estimation of lidar ratio is essential to solve the lidar equation and important in the study of climatic impact of aerosols.

Many researchers have reported the lidar ratio estimation as a part of retrieval of extinction and backscatter profiles of tropospheric aerosols using ground as well as satellite data. Takamura et al. (1994) derived lidar ratio combining the measurements from lidar, sunphotometer and optical particle counter. Lidar ratio can be directly estimated using the Raman lidar. Ansmann et al. (2002) demonstrated that the lidar ratio retrieved using Raman lidar can be used to retrieve extinction profiles of the aerosols using elastic backscatter lidar. The National Aeronautics and Space Administration's (NASA's) Cloud-Aerosol Lidar with Orthogonal Polarisation (CALIOP) on-board Cloud-Aerosol Lidar and Infrared Pathfinder Satellite Observations (CALIPSO) launched in 2006 is the only available source of satellite data to retrieve vertical profiles of tropospheric aerosols. CALIOP is an elastic backscatter lidar (Hunt et al. 2009) that records the backscattered photon counts due to tropospheric aerosols and the vertical extinction and backscatter profiles of aerosols are retrieved solving the single scattering lidar equation (Young and Vaughan 2009). This retrieval process uses a look-up table approach for lidar ratio in order to solve the lidar equation. The lidar ratio selection scheme used for CALIOP-CALIPSO products is based on cluster analysis of aerosol measurements using data recorded at several AERONET network stations spread across the globe (Omar et al. 2009, Young and Vaughan 2009). Thus, a novel theoretical approach is presented in this paper to retrieve the lidar ratio for CALIOP-CALIPSO aerosol models.

The lidar ratio depends on two optical properties viz. extinction coefficient and backscattering coefficient and thus, it depends on the incident wavelength, refractive index and the size distribution of the aerosols. In real atmospheric conditions, aerosols exhibit different shapes and sizes and are composed of various kinds of compounds. In addition to this, various aerosol components are affected due to variations in relative humidity. Thus, it is essential to study the variations in lidar ratio due to different atmospheric conditions for various compositions of aerosols. Salemink et al. (1984) reported a linear increase in the lidar ratio when relative humidity was increased from 40% to 80% during a field experiment details of which are not mentioned in the paper. Ackermann (1998) has reported a numerical study of lidar ratio with respect to variations in relative humidity for Nd:YAG wavelengths for continental, maritime and desert aerosol models where author has considered some hypothetical cases for number mixing ratios of the aerosol components. He has established a non-linear relationaship between relative humidity and lidar ratio. Zhao et al. (2017) used Mie theory and k-Kohler theory to study the influences of aerosol hygroscopic growth on lidar ratio and used *in-situ* data collected during a field campaign to establish a relationship between lidar ratio and relative humidity. Dusing et al. (2021) has also established a non-linear relationship between lidar ratio and relative humidity for Central European aerosols using *in-situ* data. Optical properties of aerosols are important to study the radiation balance of the Earth and climate change. Optical Properties of Cloud and Aerosols (OPAC) software tool facilitates with the dataset of optical properties of the aerosols and clouds and a program to extract these datasets. The standard global aerosol models are considered in OPAC as given in d'Almeida et al. (1991) and Hess et al. (1998). Component mixing in aerosols is based on particle number densities, which are independent of relative humidities in OPAC. However, this will affect the aerosol lidar ratio.

Several authors have reported different lidar ratio values for different aerosol models using a variety of methodologies. d'Almeida et al. (1991) have reported values of 16-22 sr for clean marine and desert models at ruby wavelength when lidar ratio was estimated as ratio of extinction coefficient to phase function at 180°. They

have reported a value up to 80 sr for Antarctic aerosols at ruby wavelength. Anderson et al. (2000) have showed a variation of 8 to 95 sr in lidar ratio values for polluted continental model at 532 nm using nephelometer data. Omar et al. (2009) have reported lidar ratio values for desert, smoke, clean continental, polluted continental, clean marine and polluted dust aerosols at 532 nm and 1064 nm varying between 20-70 sr using AERONET data. These values are reported with 30% uncertainty and are selected as lidar ratio in CALIPSO-V1 operational algorithms. The lidar ratios for polluted dust aerosols are updated to 55 sr and 48 sr at 532 nm and 1064 nm, respectively, in CALIPSO-V3 operational algorithm whereas lidar ratio for clean continental aerosols is updated to 53 sr at 532 nm in CALIPSO-V4 operational algorithm (Kim et al. 2018). Lopes et al. (2013) have reported a regional study in Brazil about lidar ratio selection algorithm for CALIPSO data only at 532 nm using AERONET sun photometers. They have reported the similar values for all aerosol models as used in CALIPSO-V1 algorithm by Omar et al. (2009) except for polluted dust in which case the lidar ratio value is updated to 55 sr. Li et al. (2022) have assessed CALIPSO-V4 lidar ratio selection algorithm by retrieving lidar ratios as combination of CALIPSO columnar attenuated backscatter and Synergised Optical Depth of Aerosols (SODA) algorithms. This study has ignored clean continental aerosols and has proposed elevated smoke and dusty marine aerosol models with lidar ratios of 47 sr and 32 sr, respectively; during night at 532 nm.

The present study reports a theoretical approach for estimation of lidar ratio from various sources, such as aerosol models reported by Hess et al. (1998) (OPAC aerosol models), Omar et al. (2005 and 2009) for wavelengths 532 nm, 673 nm and 1064 nm (CALIPSO and AERONET aerosol models). The variation in lidar ratio with respect to relative humidity was also studied at Nd:YAG wavelengths using OPAC (Hess et al. 1998) aerosol models. Hess et al. (1998) have reported aerosol models as composition of various components contributing to different aerosol types whereas Omar et al. (2005 and 2009) have reported aerosol models in terms of contribution from fine and coarse particles i.e. in terms of aerosol sizes. As mentioned earlier, theoretical approach for lidar ratio estimation using Mie theory is still a gap area for CALIPSO and OPAC aerosol models and thus, this study attempts to provide a physics based theoretical approach covering all types of aerosol models over the varying lidar ratio values based on in-situ measurements.

The paper is organised into five sections. The first section presents the introductory literature review and motivation behind this study. The second section outlines the data used in this study. The detailed methodology and Mie theory for lidar ratio estimation is presented in the third section of this paper. The results are discussed in the fourth section whereas the concluding remarks are listed in the fifth section of this paper.

2   Input Data:

The lidar ratio depends on aerosol size distribution, refractive index and incident wavelength. The inputs used in this study are the aerosol models provided in d'Almeida et al. (1991), Ackermann (1998), Hess et al. (1998), and Omar et al. (2005 and 2009).

Table 1 and 2 present the CALIOP-CALIPSO aerosol models and cluster classified AERONET aerosol models, respectively; defined in Omar et al. (2009 and 2005) at 532 nm, 673 nm and 1064nm. These data include the refractive indices (in terms of real part (m_r) and imaginary part (m_i)) for each of the component aerosols along with the size distribution of the aerosol in terms of median radius (r_m) and standard deviation (σ).

114 Omar et al. (2005) have reported aerosol refractive indices at 673 nm and have classified aerosols through cluster

115 analysis in six different categories numbered 1-6 viz. desert dust, biomass burning, rural, industrial pollution,

116 polluted marine and dirty pollution using AERONET data. The desert dust and polluted marine (i.e. category 1

117 and category 5) aerosol models represent the categories of aerosols originated from the natural sources whereas

118 the biomass burning, continental pollution and dirty pollution (i.e. category 2, 4, and 6) aerosol models represent

119 the aerosols emanating from the anthropogenic sources. Rural background aerosol model (i.e. category 3)

120 represent those aerosols which are observed in relatively clean atmosphere.

121 The category 1 aerosols have fine fraction by volume of 0.22 indicating that coarse particles dominate the volume

122 of this category. The median radius and geometric standard deviation for the fine mode is of 0.12 µm and 1.48,

123 respectively; for this category. The refractive index of this category of aerosols is considered to be $1.45 - 0.0036i$

124 as reported in table 2. The sites considered for these category of aerosols are either desert regions, close to desert

125 regions or the sites where desert dust has been observed as a result of long-range transport. The category 2 aerosols

126 have fine fraction by volume of 0.33 whereas median and geometric standard deviation for the fine mode is 0.14

127 µm and 1.56, respectively. Category 2 aerosols are dominated by coarse mode particles which have a median

128 radius and geometric standard deviation of 3.73 µm and 2.14, respectively. Category 1 and category 2 aerosols

129 have single scattering albedo values of 0.94 and 0.82, respectively which are estimated using Mie theory presented

130 in this paper. These single scattering albedo values are consistent with those reported by Omar et al. (2005).

131 Category 3 aerosols are characterised by low optical depth values as they are originated from clean atmosphere.

132 These aerosols have fine fraction by volume of 0.38 indicating dominance of coarse particles. The median radius

133 and geometric standard deviation for the fine mode is of 0.13 µm and 1.50, respectively. The refractive index for

134 this category of aerosols is considered to be $1.45 - 0.0092i$. The single scattering albedo value is observed to 0.89

135 for category 3 aerosols. The category 4 aerosols are found in urban centres or near urban centres and are dominated

136 by the natural pollutants such as sulfate particles (Omar et al. 2005). The refractive index for these category of

137 aerosols is considered to be $1.41 - 0.0063i$ which is representing the natural pollutants comprising category 4

138 aerosols. The size distribution of category 4 aerosols is described by a median radius and geometric standard

139 deviation for fine mode of 0.16 µm and 1.53, respectively. The median radius and geometric standard deviation

140 for coarse mode is of 3.55 µm and 2.07, respectively. The single scattering albedo for these category of aerosols

141 is estimated to be 0.93.

142 The category 5 aerosols are observed at islands or at coastal regions. The fine fraction by volume is of 0.26 and

143 size distribution is described by a median radius and geometric standard deviation for fine mode of 0.17 µm and

144 1.61, respectively. The refractive index for these category of aerosols is considered to be $1.39 - 0.0044i$. These

145 optical properties are resulted in the single scattering albedo of 0.94 for polluted marine aerosols. The category 6

146 aerosols are similar to category 4 aerosols with a high imaginary part of refractive index. The refractive index of

147 category 6 aerosols is considered to be $1.41 - 0.0337i$ which resulted in low single scattering albedo of 0.68. The

148 low single scattering albedo indicates that these are the aerosols with mostly carbon element in it (Omar et al.

149 2005). The size distribution of these category of aerosols is described by a median radius and geometric standard

150 deviation of 0.14 µm and 1.54, respectively. The more details about these six categories of aerosols can be found

151 in Omar et al. (2005).

152   The theoretically derived lidar ratios were compared with lidar ratio derived using AERONET data for three

153   different stations classified for each of the above-mentioned six categories. The details are discussed in results

154   section of this paper.

155   Table 3, 4 and 5 collectively report the OPAC aerosol models. These aerosol models are defined in terms of their

156   size distribution with respect to relative humidity, refractive indices at 532 nm and 1064 nm and composition of

157   aerosol types in terms of number mixing ratio (μ). The lognormally distributed aerosol components were

158   considered in this study. The relative humidity was varied from 0% to 99% with intermediate steps at 50%, 70%,

159   80%, 90% and 98%. The details about OPAC aerosol models can be found in Hess et al. (1998).

160   **3   Computation of Lidar Ratio using Mie Theory:**

161   In this study, the aerosols were assumed as homogeneous isotropic spheres scattering the electromagnetic

162   radiation incident upon them. These scattering phenomenons are modelled using Mie theory, which is discussed

163   in Bohren and Huffman (1983) and Vermote et al. (2006) and many other authors. The lidar ratio, which is defined

164   as the ratio of extinction coefficient to backscattering coefficient, is derived in the present study using the Mie

165   theory equations. The computational equations are presented here briefly, for the ready reference.

166   The Mie parameter (x) for an aerosol with refractive index, $m = m_r - im_i$; is defined as

167     $$x = \frac{2\pi r}{\lambda},$$ (1)

168   where r is the aerosol particle radius in micron and λ is the wavelength in micron. Here m is the refractive index

169   with real part m_r and imaginary part m_i.

170   Two complex functions $S_1(x, m, \theta)$ and $S_2(x, m, \theta)$ related to amplitude of scattered radiation that are

171   perpendicular and parallel to the plane of scattering with scattering angle θ, respectively, can be defined as

172   follows.

173     $$S_1(x, m, \theta) = \sum_{n=1}^{\infty} \frac{(2n+1)}{n(n+1)} [a_n(x, m)\pi_n(cos\theta) + b_n(x, m)\tau_n(cos\theta)] \text{ and }$$ (2)

174     $$S_2(x, m, \theta) = \sum_{n=1}^{\infty} \frac{(2n+1)}{n(n+1)} [a_n(x, m)\tau_n(cos\theta) + b_n(x, m)\pi_n(cos\theta)],$$ (3)

175   where, the complex functions $a_n(x, m)$ and $b_n(x, m)$ are given by

176     $$a_n(x, m) = \frac{\Psi'_n(mx)\Psi_n(x) - m\Psi_n(mx)\Psi'_n(x)}{\Psi'_n(mx)\xi_n(x) - m\Psi_n(mx)\xi'_n(x)} \text{ and }$$ (4)

177     $$b_n(x, m) = \frac{m\Psi'_n(mx)\Psi_n(x) - \Psi_n(mx)\Psi'_n(x)}{m\Psi'_n(mx)\xi_n(x) - \Psi_n(mx)\xi'_n(x)},$$ (5)

178   which are defined in terms of Ricatti-Bessel functions $\Psi_n(z = x \text{ or } mx)$ and $\xi_n(z = x \text{ or } mx)$. Ricatti-Bessel

179   functions are evaluated using their logarithmic derivatives details of which are provided in Vermote et al. (2006).

180   In order to compute the complex functions $S_1(x, m, \theta)$ and $S_2(x, m, \theta)$, the functions π_n and τ_n are computed

181   using associated Legendre polynomials. The functions π_n and τ_n are the functions of scattering angle θ. These

182   can be computed using the recurrence relations

183     $$n\pi_{n+1}(cos\theta) = (2n + 1)cos\theta\pi_n(cos\theta) - (n + 1)\pi_{n-1}(cos\theta) \text{ and }$$ (6)

184     $$\tau_{n+1}(cos\theta) = (n + 1)cos\theta\pi_{n+1}(cos\theta) - (n + 2)\pi_n(cos\theta).$$ (7)

185   which are initialised with $\pi_0(cos\theta) = 0$, $\pi_1(cos\theta) = 1$, and $\tau_0(cos\theta) = cos\theta$.

Using these quantities, the extinction efficiency ($Q_e(\lambda, r, m)$), dimensionless angular-scattering intensity efficiency ($M_{11}(\lambda, r, m, \theta)$), the scattering efficiency ($Q_{sca}(\lambda, r, m)$), and backscattering efficiency ($Q_{back}(\lambda, r, m)$) can be computed as

$$Q_e(\lambda, r, m) = \frac{\sigma_e(\lambda, r, m)}{\pi r^2} = \frac{2}{x^2} \sum_{n=1}^{\infty} (2n+1) \mathcal{R}e[a_n(x, m) + b_n(x, m)], \tag{8}$$

$$M_{11}(\lambda, r, m, \theta) = \frac{1}{2x^2}[S_1(x, m, \theta)S_1^*(x, m, \theta) + S_1(x, m, \theta)S_2^*(x, m, \theta)], \tag{9}$$

$$Q_{sca}(\lambda, r, m) = \frac{\sigma_{sca}(\lambda, r, m)}{\pi r^2} = \frac{2}{x^2} \sum_{n=1}^{\infty}(2n+1)[a_n(x, m)a_n^*(x, m) + b_n(x, m)b_n^*(x, m)] \text{ and} \tag{10}$$

$$Q_{back}(\lambda, r, m) = \frac{4}{x^2}|S_1(x, m, 180^0)|^2 = 4M_{11}(\lambda, r, m, 180^0), \tag{11}$$

where r is the particle radius, $\sigma_e(\lambda, r, m)$ is the extinction cross section and $\sigma_{sca}(\lambda, r, m)$ is the scattering cross section.

Thus, the lidar ratio can be computed as

$$LR = \frac{Nr}{Dr} = \frac{\sum_{i=1}^{M} \int_0^{\infty} Q_e(\lambda, r, m_i) \pi r^2 n(r) dr}{\sum_{i=1}^{M} \int_0^{\infty} Q_{back}(\lambda, r, m_i) \pi r^2 n(r) dr}. \tag{12}$$

The single scattering albedo can be computed as

$$\omega_0 = \frac{\sum_{i=1}^{M} \int_0^{\infty} Q_{sca}(\lambda, r, m_i) \pi r^2 n(r) dr}{\sum_{i=1}^{M} \int_0^{\infty} Q_e(\lambda, r, m_i) \pi r^2 n(r) dr}. \tag{13}$$

In this study, an aerosol is considered as mixture of its constituent components. And each of the component is lognormally distributed with median radius r_m and standard deviation σ. Thus,

$$n(r) = \frac{\mu N_{tot}}{\sqrt{2\pi} r ln(\sigma)} exp\left[-\frac{ln^2(r/r_m)}{2ln^2\sigma}\right], \tag{14}$$

where μ is the number mixing ratio (i.e. normalised number particle concentration) and N_{tot} is the total number density of the aerosol component.

The relative humidity influences the refractive index of the hygroscopic aerosol components and the effective refractive index is

$$m_i = m_w + (m_{0,i} - m_w)\left(\frac{r_{0,i}}{r_{m,i}}\right)^3, \tag{15}$$

where m_w is the refractive index of the water, $m_{0,i}$ is the refractive index of the dry particle of component i and $r_{0,i}$ is the median radius of the dry particle of component i.

The theory presented above is with the assumption of homogenous spherical isotropic aerosol particles, which simplifies the computation of lidar ratio. However, if the particles are not homogenous and anisotropic then the above theory may cause errors as the scattering phase function will differ to address the anisotropy. Moreover, if the particles are nonhygroscopic especially when the particles are large as compared to the incident wavelength then the above theory fails (Ackermann 1998).

4   Results and Discussion:

4.1 Lidar Ratio for AERONET and CALIPSO Aerosol Models defined in terms of particle sizes:

The aerosol models defined in terms of particle size by Omar et al. (2005 and 2009) were used to estimate the lidar ratio for aerosol models used in operational algorithms of CALIOP-CALIPSO. Omar et al. (2005) used cluster analysis for AERONET data to define the aerosol models at 673 nm. Table 6 shows the lidar ratio estimated using the Mie theory for each of the six clusters defined by Omar et al. (2005). The maximum lidar ratio of 48.87

sr was observed for dirty pollution type of aerosols whereas the minimum of 28.76 sr was observed for desert dust kind of aerosols. The lidar ratios at 532 nm are mostly discussed in literature (Ackermann 1998, Anderson et al. 2000, Omar et al. 2009, Lopes et al. 2013 and Kim et al. 2018 and 2022) and scanty literature is available for lidar ratios at 673 nm. Moreover, these aerosol models are derived using AERONET data. Thus, the estimated lidar ratios at 673 nm were compared with those of the AERONET data.

The data for three different stations for each of the category was selected and aerosol lidar ratio was computed using equation (12) as a multiplier of 4π. Tables 7-12 show the statistics of the lidar ratio for different AERONET stations belonging to different categories. The daily averages of the lidar ratios were obtained using the AERONET single scattering albedo and phase function values and were compared with the Mie theory estimated values. The Mie theory estimated values were observed to comply with the observed values of lidar ratios using AERONET data as the theoretically estimated values were lying in between the minimum and maximum of the daily lidar ratio values. The differences in the theoretical values estimated using Mie theory and those observed using AERONET data were primarily due to the refractive indices of the different aerosol types present at the different AERONET stations. Omar et al. (2005) had classified the different aerosol types mentioned in section 2 using cluster analysis and the geographical location of these AERONET stations was also considered to be an important factor while classification. Thus, the composition of the aerosols observed over a period of time varied resulting in the variation of the refractive indices. The theoretically computed lidar ratios were based on the refractive index of the centre of the cluster analysed using AERONET data before 2002 (Omar et al. 2005) whereas the AERONET stations data used in this study spanned over 1998 to 2021 leading to the differences in the refractive indices of the aerosol types. The shape of the aerosol particles, their size distribution and their particle density present in the atmosphere may be the secondary reasons for the differences between the theoretically estimated values of lidar ratio using Mie theory and the lidar ratio computed using AERONET stations data which needs further investigation.

The aerosol models derived using the cluster analysis by Omar et al. (2005) and their respective lidar ratios were used in lidar ratio selection and feature detection algorithm of CALIOP-CALIPSO (Young and Vaughan 2009). These aerosol models and their respective lidar ratios used in operational algorithms of CALIOP-CALIPSO are specified in Young and Vaughan (2009). These lidar ratios were subsequently updated in the V3 and V4 CALIOP-CALIPSO operational algorithms (Kim et al. 2018). The basis for lidar ratio selection algorithm for CALIOP-CALIPSO operational products has been the cluster analysis using the AERONET data and thus, the lidar ratios were estimated using Mie theory, which gives the physical basis for the lidar ratio selection algorithm.

Figure 1 and 2 show the distribution of extinction and backscattering coefficients for CALIPSO aerosol models at 532 nm and 1064 nm; respectively. The particle sizes were varied from 0.01 μm to 5 μm and the cut-off radius for fine particles was taken to be 1 μm for all CALIPSO aerosol models except clean marine aerosols in which case the fine particle radius cut-off was 0.6 μm. The maxima of extinction and backscattering coefficients at 532 nm and 1064 nm, for all aerosol models except clean marine aerosols was observed between 0.07 μm to 0.4 μm. In case of all aerosol models, it was observed that the contribution from fine particles was more in magnitude compared to that from coarser particles at 532 nm and 1064 nm except the clean marine model. In case of clean marine aerosols at 1064 nm, the coarser particles were observed to contribute significantly in magnitude to the extinction coefficient as compared to fine particles producing lidar ratio value of 71 sr.

259   Table 13 shows the lidar ratio values estimated for the CALIPSO aerosol models specified in Omar et al. (2009)
260   and its comparison with the lidar ratio values selected in various versions of CALIOP-CALIPSO operational
261   algorithms. It was observed that the lidar ratio values estimated using Mie theory in present study comply with
262   the lidar ratio values reported in literature for CALIPSO operational algorithms. Omar et al. (2006) reported that
263   the lidar ratio for dust aerosols vary between 10 sr to 146 sr when AERONET stations data was classified using
264   cluster analysis. However, the lidar ratio value for dust aerosols proposed in this study at 1064 nm is lower than
265   that used in the CALIPSO V4 operational algorithm. In case of desert dust particles at 1064 nm the variation up
266   to 31 sr was allowed in CALISPO V4 operational algorithm, whereas the present study proposed lidar ratio value
267   of 20 sr for desert dust aerosols at 1064 nm. The desert dust lidar ratio at 1064 nm proposed for CALIPSO aerosol
268   model was observed to be consistent with OPAC desert aerosol model in which case lidar ratio was observed to
269   be centred on 23 sr. These results for desert aerosols at 1064 nm comply with those reported by Ackermann (1998)
270   where dry desert aerosol lidar ratio was lying just under 20 sr. The results for OPAC aerosol models are discussed
271   in detail in the subsequent section. The dust aerosol lidar ratio values at 532 nm and 1064 nm was defined using
272   discrete-dipole approximation (DDA) technique in CALIPSO operational algorithm initially (Omar et al. 2009).
273   The DDA technique considers the non-sphericity of the dust particles (Kalashnikova and Sokolik 2002), whereas
274   Mie theory is quite applicable to spherical homogeneous particles. Thus, the lidar ratio value at 1064 nm was
275   observed to be underestimated using Mie theory, which was also reported by Cattrall et al. (2005). Shin et al.
276   (2018) have reported that the dust lidar ratio at 1020 nm was centred at 44 sr, 40 sr, 54 sr, 36 sr, and 35 sr at Gobi,
277   Arabian, Saharan, Great Basin and Great Victoria deserts, respectively. The dust lidar ratio at 1064 nm has thus
278   showed a large variation temporally and geographically, and thus encouraging the utility of proposed value of
279   dust lidar ratio for retrieval of aerosol optical properties using CALIPSO data.
280   The lidar ratio proposed for clean continental model at 532 nm in CALIPSO V4 operational algorithm was 53 $\pm$
281   24 sr, allowing the variation up to 77 sr. The Mie theory estimate for clean continental model at 532 nm was
282   centred on 85 sr considering the refractive index of the centre cluster as provided in Omar et al. (2009). This lidar
283   ratio value for clean continental aerosol model was observed to be consistent with those reported in literature.
284   Omar et al. (2006) have reported that the clean continental lidar ratio value varied between 10 sr to 149 sr when
285   estimated using AERONET stations data and Nehrir et al. (2011) have reported the variation in clean continental
286   lidar ratio of 55 − 95 sr at 532 nm observed at Bozeman, Montana. The high value of lidar ratio at 532 nm for
287   clean continental aerosols was observed due to high absorption by fine sub-micron (particles with radius < 0.5
288   μm) particles. The variation in refractive index will also affect the lidar ratio value, which was evident when
289   compared to OPAC aerosol models where the lidar ratio of clean continental aerosols was centred on 53 sr. Similar
290   results were observed in case of clean marine aerosols at 532 nm.
291   The theoretically proposed value in the present study for clean marine aerosols at 532 nm was 57.31 sr. The
292   absorption by the fine particles at 532 nm leads to the high value of lidar ratio. The theoretically estimated lidar
293   ratio for clean marine aerosols at 532 nm was observed to be consistent with that reported in the literature. Masonis
294   et al. (2003) have measured the clean marine aerosol lidar ratio as 60.1 sr at 532 nm during Shoreline Environment
295   Aerosol Study (SEAS) experiment. Dawson et al. (2015) have reported a variation of 10 − 90 sr in the lidar ratio
296   of clean marine aerosols. Li et al. (2022) reported the median value of lidar ratio for clean marine aerosols of 60
297   sr at 532 nm. Li et al. (2022) have measured a peak value of 55 sr at 532 nm over Bay of Bengal. CALISPO
298   operational V3 algorithm allowed variation up to 68 sr in lidar ratio of clean marine aerosols at 1064 nm whereas

299 the present study estimated the value of 71 sr for clean marine aerosols at 1064 nm. This high lidar ratio value for

300 clean marine particles at 1064 nm was due to scattering by coarse super-micron (particles with radius > 0.5 μm)

301 particles, which was observed to be consistent as reported in Masonis et al. (2003). Thus, the Mie theory estimated

302 lidar ratio values can provide the physical basis for the CALIPSO operational algorithms and can be used as look-

303 up table to derive the vertical extinction and backscatter particulate profiles using satellite data.

304 The theoretical approach proposed in this study to estimate lidar ratio for CALIPSO aerosol models was further

305 validated through estimation of single scattering albedo at 673 nm for the aerosol models classified using

306 AERONET data as described in table 2. The single scattering albedo values for AERONET aerosol models viz.

307 Category 1 to Category 6 were estimated using the above presented Mie theory as 0.94, 0.82, 0.89, 0.93, 0.94 and

308 0.68, respectively. The single scattering values at 673 nm for these AERONET aerosol models viz. Category 1 to

309 Category 6 were reported by Omar et al. (2005) as 0.93, 0.80, 0.88, 0.92, 0.93 and 0.72. The comparison between

310 the theoretically estimated and literature reported single scattering albedo values showed the percent absolute

311 difference between 1.06% to 5.56%, which validates the proposed Mie theory for estimation of lidar ratio.

4.2 Lidar Ratio for OPAC Aerosol Models Defined in terms of Constituent Components:

313 The lidar ratios were also estimated when aerosol models were specified in terms of different constituent

314 compositions as used in OPAC. The aerosol models viz. clean continental, average continental, polluted

315 continental, urban, clean maritime, maritime tropical, polluted maritime, desert, arctic and antarctic were used in

316 the present study to estimate the lidar ratio using Mie theory. The number mixing ratios as specified in OPAC

317 software by Hess et al. (1998) were used in the present study to define the size distribution of aerosols. The relative

318 humidity causes an increase in size of a hygroscopic particle such as water soluble, sea salt and sulfate particles.

319 Thus, the backscattering and extinction profiles of these particles are significantly affected.

320 Figure 3 shows the variation in backscattering coefficient of the continental and maritime aerosols at 532 nm and

321 1064 nm. The backscattering coefficient of continental and maritime aerosols were observed to increase when

322 relative humidity was increased from 0% to 99%. The increase in backscattering with relative humidity was

323 considerably higher in clean continental and clean maritime aerosols as compared to polluted continental, urban

324 and polluted maritime aerosols at 532 nm and 1064 nm. Clean maritime and tropical maritime aerosols were

325 observed to have equivalent backscattering coefficients due to their equivalent composition of water soluble and

326 sea salt particles.

327 Figure 4 shows the variation in backscattering coefficients of the desert, arctic and antarctic aerosol models at 532

328 nm and 1064 nm. The Antarctic aerosols showed a sharp and significant increase in their backscattering

329 coefficients at 532 nm and 1064 nm. The increase in backscattering coefficients was observed to be more at 1064

330 nm compared to 532 nm. According to Figure 6 (c), both wavelengths show an increase in lidar ratio, but 532 nm

331 has a more significant increase than 1064 nm. In addition, the lidar ratio values are lower at 1064 nm than at 532

332 nm.   Increase in backscattering coefficient with relative humidity at 532 nm and 1064 nm will cause increase or

333 decrease in lidar ratio with respect to relative humidity depending upon the rate at which the extinction and

334 backscattering coefficients are increasing or decreasing.

335 The variation in lidar ratios of continental and maritime aerosol models with reference to relative humidity at 532

336 nm and 1064 nm is as shown in Figure 5. The lidar ratio showed an increase in values for polluted continental and

337 polluted maritime aerosols over the clean continental and clean maritime aerosols. This increase was mainly

observed due to greater contribution of soot particles in the polluted aerosols. Soot particles are sub-micron absorbing particles. Thus, with increasing number mixing ratio of soot particles in the polluted aerosols as compared to clean aerosols, the extinction coefficient increases leading to increase in lidar ratio values of polluted aerosols. An increase in lidar ratio values was observed at 532 nm and 1064 nm when relative humidity was increased from 80% to 99% in all types of continental and maritime aerosols, primarily due to increase in the size of water soluble particles. The decrease in lidar ratio when relative humidity was increased from 0% to 80% was observed due to decrease in lidar ratio of the water soluble particles which are hygroscopic in nature. This decrease was primarily due to significant decrease in the imaginary part of the refractive index of water soluble component due to relative humidity. The decrease in the imaginary part of refractive index of water soluble particles leads to decrease in absorption As a result, the rate at which extinction coefficient increases is either less than or equivalent to the rate at which backscattering coefficient increases. This results in the decrease in lidar ratio of aerosols when RH is increased from 0 to 80%. The increase in lidar ratio from 80% to 99% is primarily due to increase in size of water soluble particles. Continental and Maritime aerosols are dominated by water soluble particles as defined in OPAC and thus an initial decrease and a gradual increase in lidar ratio values was observed at 532 nm and 1064 nm when relative humidity was increased from 0% to 99%.

The lidar ratio values of the clean continental model and clean maritime aerosol models at 532 nm and 1064 nm where observed to be centred around 53 sr to 51 sr with varying relative humidity. This is mainly because of the composition of aerosol models as defined in OPAC. In both, clean continental and clean maritime models, water soluble particles were dominant which are smaller in size as compared to the sea salt particles. However, in OPAC the number mixing ratio of sea salt particles which are coarser particles, is very low as compared to finer water soluble particles; which is not the case in CALIPSO clean marine aerosol model. In CALIPSO clean marine model, though coarser particles are more in proportion their contribution to the backscattering and extinction coefficient was observed to be less in magnitude as compared to the fine particles at 532 nm. Thus, the resulting lidar ratio values for CALIPSO aerosol model were centred on 57 sr at 532 nm, which was consistent with the results for OPAC clean maritime aerosol model.

The urban aerosols showed a significant increase in the lidar ratio values at 532 nm and 1064 nm compared to other continental aerosols. The dry urban aerosols showed a lidar ratio of 74.88 sr and 61.73 sr at 532 nm and 1064 nm, respectively; whereas dry clean continental aerosols exhibited the lidar ratio of 53.59 sr and 23.9 sr at 532 nm and 1064 nm, respectively. This significant increase in lidar ratio values of urban aerosols is primarily due to scattering soot particles. Insoluble particles hardly have any impact on lidar ratio values of urban and continental aerosols due to their very small composition. Similar results were observed when polluted maritime particles were compared to the clean maritime particles.

The variation in lidar ratios of desert, arctic and antarctic aerosols with respect to relative humidity is as shown in Figure 6. The lidar ratio values at 532 nm were observed to be greater than those at 1064 nm values for desert and antarctic aerosols. The dry desert dust lidar ratio at 532 nm was observed to be 55.32 sr. This result comply with the values for desert dust lidar ratio at 532 nm reported in literature by Muller et al. (2007), Omar et al. (2009), Kim et al. (2018) and Li et al. (2022). The lidar ratio values showed a decrease with relative humidity except the lidar ratio values of antarctic aerosols at 532 nm and 1064 nm. The model of arctic aerosols that is used in the present study is for spring season when the arctic aerosols are mainly the soot particles. Thus, a decrease in lidar

377 ratio values with relative humidity was observed in arctic aerosols as it was in polluted continental and urban

378 aerosols at 1064 nm.

379 The lidar ratio of dry Antarctic aerosols was observed to be 57.73 sr at 532 nm and 20.90 sr at 1064 nm. The

380 summertime model of Antarctic aerosols as defined in OPAC was used in the present study where the Antarctic

381 aerosols are dominated by the sulfate particles (d'Almeida et al. 1991, Hess et al. 1998). Sulfate particles are

382 hygroscopic in nature with significant large sizes as compared to water soluble particles. The imaginary part of

383 refractive index of sulfate particles in considerably small as compared to water soluble particles at 532 nm and

384 1064 nm. Thus, a sharp increase in lidar ratio of sulfate particles was observed when relative humidity was

385 increased from 0% to 99% as opposed to continental, maritime and desert aerosol models.

386 **5   Conclusions:**

387 This paper presented a complex theoretical approach for estimating lidar ratio through Mie theory using CALIPSO

388 and OPAC aerosol models. The lidar ratios were estimated at three wavelengths viz. 532 nm, 673 nm and 1064

389 nm. Mie theory estimated lidar ratios at 673 nm were compared with AERONET data-derived lidar ratios at 675

390 nm and Mie theory estimated lidar ratios at 673 nm were observed to lie between the minima and maxima of the

391 AERONET data-derived lidar ratios at 675 nm. Mie theory estimated lidar ratio values for CALIPSO aerosol

392 models were in good agreement with those reported in literature for CALIPSO operational algorithm. Thus,

393 theoretically estimated lidar ratios for CALIPSO aerosol models may be used in future for CALIPSO operational

394 algorithms. CALIPSO aerosol models were specified in terms of number mixing ratio of the fine and coarse

395 particles instead of component particle type and fine particles were observed to have more significant contribution

396 towards extinction and backscattering coefficient despite their low mixing ratio as compared to coarse particles.

397 Thus, Mie theory derived lidar ratio values provide the physical basis for the lidar ratio selection algorithm for

398 derivation of vertical extinction and backscatter particulate profiles using CALIPSO data.

399 The dependence of lidar ratio with relative humidity was analysed using OPAC aerosol models including Arctic

400 and Antarctic aerosols where each aerosol type was identified with the corresponding number mixing ratio of the

401 component particles. The lidar ratio was observed to decrease when relative humidity was increased from 0% to

402 80% and a gradual increase in lidar ratio was observed when relative humidity was increased further to 99%. This

403 phenomenon is the result of dominance of hygroscopic water-soluble particles constituting clean continental, clean

404 marine, tropical continental and desert aerosols. The increase in number mixing ratio of soot particles showed an

405 overall increase in the lidar ratio values of polluted continental, urban and polluted marine aerosols over clean

406 continental and clean marine particles. The soot particles dominate the urban aerosols and arctic aerosols, which

407 are non-hygroscopic fine particles. Thus, a decrease in lidar ratio of urban and arctic aerosols was observed with

408 respect to relative humidity and an increase in the backscattering coefficient of urban and arctic aerosols was

409 observed with relative humidity due to contribution from the hygroscopic water-soluble particles that grows in

410 size in presence of water vapour in the atmosphere. In case of Antarctic aerosols, the lidar ratio was observed to

411 increase with respect to relative humidity due to hygroscopic sulfate particles that backscattered heavily in

412 presence of water vapour.

413 The method presented in this study to estimate the lidar ratio using Mie theory is valid only for spherical, isotropic,

414 non-hygroscopic particles and thus there can be possible errors occurring in the lidar ratio values especially when

the aerosols are anisotropic and hygroscopic in nature. Thus, there is future scope for the present study to extend it to theoretical estimation of lidar ratio in case of hygroscopic and anisotropic non-homogeneous particles.

6   Acknowledgement:

The authors are thankful to Shri. N. M. Desai, Director-SAC (ISRO), Dr. Rashmi Sharma, DD-EPSA/SAC and Dr. B. K. Bhattacharya, GD-AESG/EPSA/SAC for their support and encouragement to carry out this work. The authors are thankful to all those who directly and indirectly supported in realisation of this activity. This research is carried out under SAC, ISRO's TDP/R&D program.

7   Competing Interests:

This is being declared that none of the authors have any competing interests.

8   References:

Ackermann, J.: The Extinction-to-Backscatter Ratio of Tropospheric Aerosol: A Numerical Study, J. Atm. Ocea. Tech., 15, 1043-1050, 1998.

Anderson, T. L., Masonis, S. J., Covert, D. S., Charlson, R. J., and Rood, M. J.: In situ measurement of the Aerosol Extinction-to-Backscatter Ratio at a Polluted Continental Site, JGR, 105, 26907-26915, 2000.

Ansmann, A., Wagner, F., Müller, D., Althausen, D., Herber, A., von Hoyningen-Huene, W., and Wandinger, U.: European Pollution Outbreaks during ACE 2: Optical Particle Properties Inferred from Multiwavelength Lidar and Star-Sun Photometry, J. Geophys. Res.-Atmos., 107, 8–14, 2002.

Bohren, C. F., and Huffman, D. R.: Absorption and Scattering of Light by Small Particles, Wiley and Sons, 530 pp., 1983.

Cattrall, C., Reagan, J., Thome, K., and Dubovik, O.: Variability of Aerosol and Spectral Lidar and Backscatter and Extinction Ratios of Key Aerosol Types Derived from Selected Aerosol Robotic Network Locations, J. Geophys. Res.-Atmos., 110, D10S11, 2005.

d'Almeida, G., Koepke, P., and Shettle, E. P.: Atmospheric Aerosols: Global Climatology and Radiative Characteristics, A. Deepak, 561 pp., 1991.

Dawson, K. W., Meskhidze, N., Josset, D., and Gasso, S.: Spaceborne Observations of the Lidar Ratio of Marine Aerosols, Atmos. Chem. Phys., 15, 3241-3255, 2015.

Dusing, S., Ansmann A., Baars, H., Corbin, J. C., Denjean, C., Gysel-Beer, M., Muller, T., Poulain, L., Siebert, H., Spindler, G., Tuch, T., Wehner, B., and Wiedensohler, B.: Measurement Report: Comparison of Airborne, in-situ Measured, Lidar-based and Modeled Aerosol Optical Properties in the Central European Background – Identifying Sources of Deviations, Atmos. Chem. Phys., 21, 16745-16773, 2021.

Hess, M., Koepke, P., and Schult, I.: Optical Properties of Aerosols and Clouds: The Software Package OPAC, Bull. Amer. Meteor. Soc., 79, 831-844, 1998.

Kalashnikova, O. V., and Sokolik, I. N.: Importance of Shapes and Compositions of Wind-blown Dust Particles for Remote Sensing at Solar Wavelengths, Geophys. Res. Lett., 29(10), 1398, 2002.

Kim, M. H., Omar, A. H., Tackett, J. L., Vaughan, M. A., Winker, D. M., Trepte, C. R., Hu, Y., Liu, Z., Poole, L. R., Pitts, M. C., Ka, J., Magill, E.: The CALIPSO version 4 Automated Aerosol Classification and Lidar Ratio Selection Algorithm, Atm. Meas. Tech., 11, 6107-6135, 2018.

Li, Z., Painemal, D., Schuster, G., Clayton, M., Ferrare, R. A., Vaughan, M. A., Josset, D., Kar, J., Trepte, C. R.: Assessment of Tropospheric CALIPSO Version 4.2 Aerosol Types over the Ocean using Independent CALIPSO-SODA Lidar Ratios, Atm. Meas. Tech., 15, 2745-2766, 2022.

Lopes, F. J. S., Landulfo, E., and Vaughan, M. A.: Evaluating CALIPSO's 532 nm lidar ratio selection algorithm using AERONET sun photometers in Brazil, Atmos. Meas. Tech., 6, 3281-3299, 2013.

Masonis, S. J., Anderson, T. L., Covert, D. S., Kapustin, V., Clarke, A. D., Howell, S., and Moore, K.: A Study of the Extinction-to-Backscatter Ratio of Marine Aerosol during the Shoreline Environment Aerosol Study, Atmos. Chem. Phys., 20, 1388-1402, 2003.

Muller, D., Ansmann, A., Mattis, I., Tesche, M., Wandinger, U., Althausen, D., and Pisani, G. : Aerosol-type-dependent Lidar Ratios Observed with Raman Lidar, JGR, 112, D16202, 2007.

Nehrir, A. R., Repasky, K. S., Reagan, J. A., and Carlsten, J. L.: Optical Characterisation of Continental and Biomass-Burning Aerosols over Bozeman, Montana: A Case Study of the Aerosol Direct Effect, J. Geophys. Res.-Atmos., 116, D201201, 2011.

Omar, A. H., Won, J. G., Winker, D. M., Yoon, S. C., Dubovik, O., and McCormick, M. P.: Development of Global Aerosol Models using Cluster Analysis of Aerosol Robotic Network (AERONET) Measurements, JGR, 110, 1-14, 2005.

Omar, A. H., Winker, D. M., and Vaughan, M. A.: Selection Algorithm for CALIPSO Lidar Aerosol Extinction-to-Backscatter Ratio, Proc. SPIE 6367, Lidar Technologies, Techniques and Measurements for Atmospheric Remote Sensing II, 63670M, 2006.

Omar, A. H., Winker, D. M., Kittaka, C., Vaughan, M. A., Liu, Z., Hu, Y., Trepte, C. R., Rogers, R. R., Ferrare, R. A., Lee, K. P., Kuehn, R. E., and Hostetler, C. A.: The CALIPSO Automated Aerosol Classification and Lidar Ratio Selection Algorithm, J. Atm. Ocea. Tech., 26, 1994-2014, 2009.

Salemink, H., Schotanus, P., and Bergwerff, J. B.: Quantitative Lidar at 532 nm for Vertical Extinction Profiles in the Lidar Solution, Appl. Phys., 34B, 187–189, 1984.

Shin, S. K., Tesche, M., Kim, K., Kezoudi, M., Tatarow, B., Muller, D., and Noh, Y.: On the Spectral Depolarisation and Lidar Ratio of Mineral Dust provided in the AERONET Version 3 Inversion Product, Atmos. Chem. Phys., 18, 12735-12746, 2018.

Takamura, T., Sasano Y., and Hayasaka T.: Tropospheric Aerosol Optical Properties Derived from Lidar, Sun Photometer, and Optical Particle Counter Measurements, Appl. Opt., 33, 7132–7140, 1994.

Vermote, E. F., Tanre, D., Deuze, J. L., Herman, M., Morcrette, J. J., Kotchenova, S. Y.: Second Simulation of a Satellite Signal in the Solar Spectrum – Vector (6SV) User Guide Version 3 – Part II, available at (http://6s.ltdri.org/), 2006.

Young, S. A. and Vaughan, M. A.: The Retrieval of Profiles of Particulate Extinction from Cloud-Aerosol Lidar Infrared Pathfinder Satellite Observations (CALIPSO) data: Algorithm Description, J. Atm. Ocea. Tech., 26, 1105-1119, 2009.

487 Zhao, G., Zhao, C., Kuang, Y., Tao, J., Tan, W., Bian, W., Li, J. and Li, C.: Impact of Aerosol Hygroscopic

488 Growth on Retrieving Aerosol Extinction Coefficient Profiles from Elastic-Backscatter Lidar Signals, Atmos.

489 Chem. Phys., 17, 12133-12143, 2017.

490

491

492
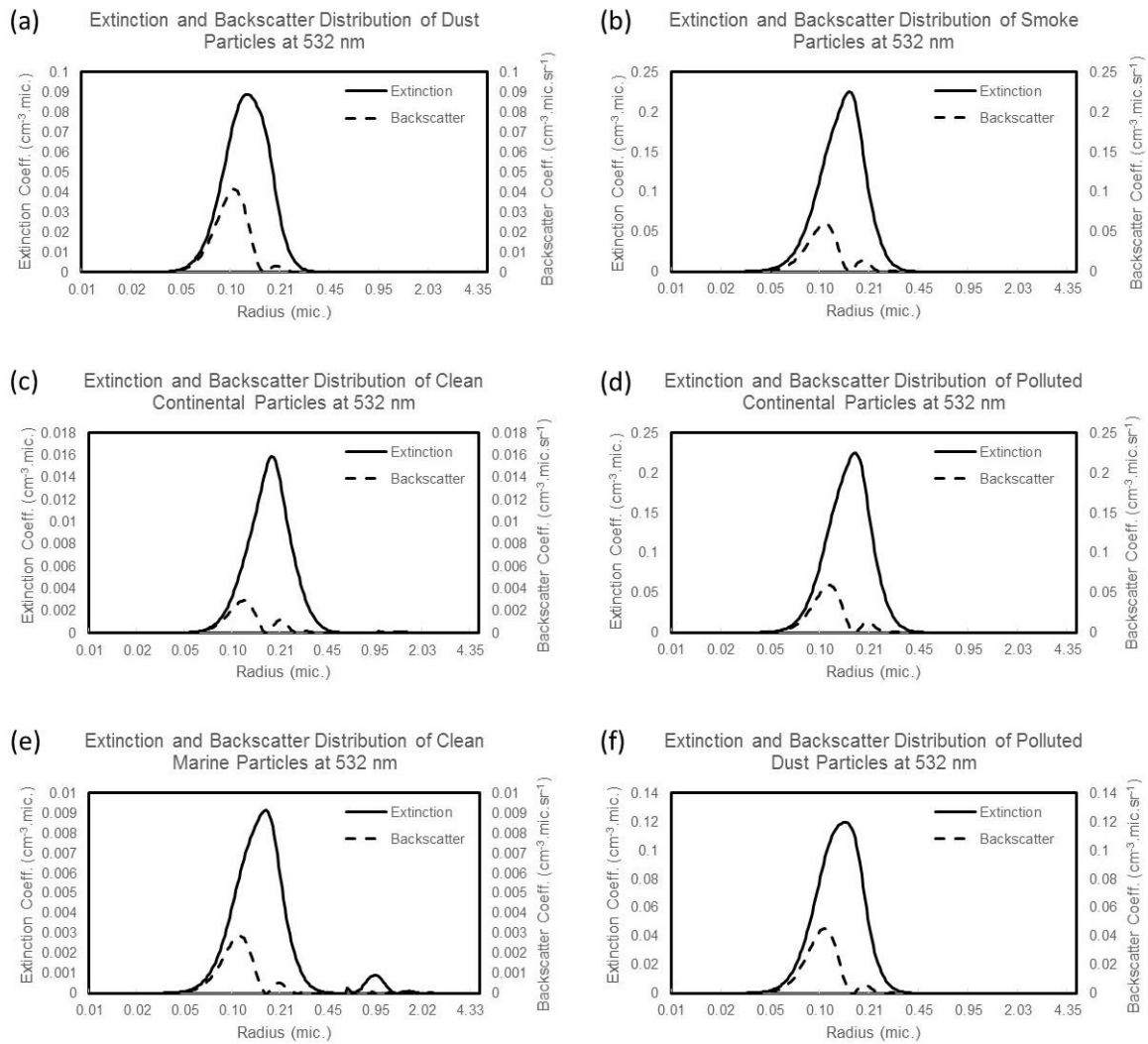
493

494

495

496 **Figure 1**: Extinction and Backscatter Distribution at 532 nm of CALIPSO Aerosol Models viz. (a) Dust (b)

497 Smoke (c) Clean Continental (d) Polluted Continental (e) Clean Marine and (f) Polluted Dust

498

499

500

501

502

503
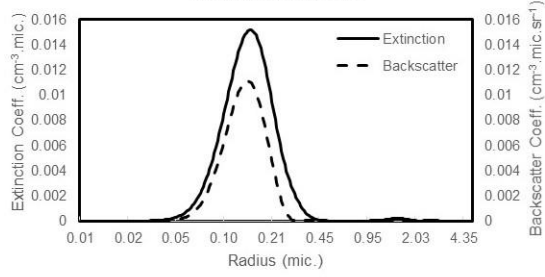
504

505

506
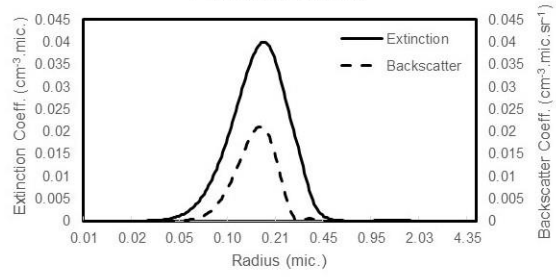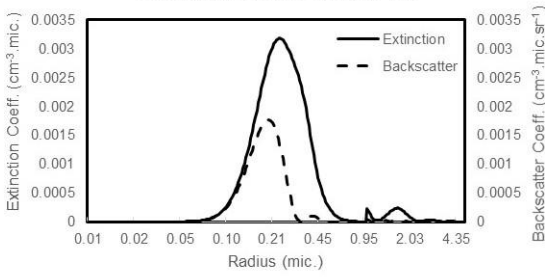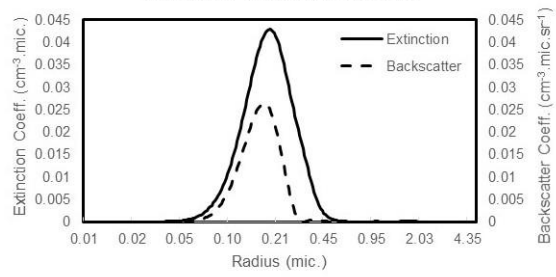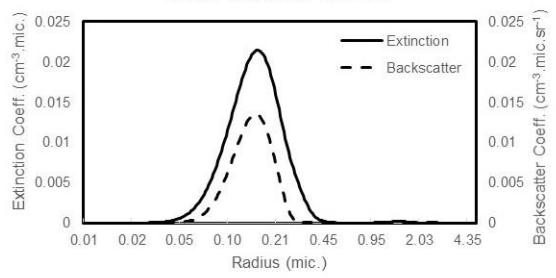
507 **Figure 2**: Extinction and Backscatter Distribution at 1064 nm of CALIPSO Aerosol Models viz. (a) Dust (b)
508 Smoke (c) Clean Continental (d) Polluted Continental (e) Clean Marine and (f) Polluted Dust

509

510

511

512

513
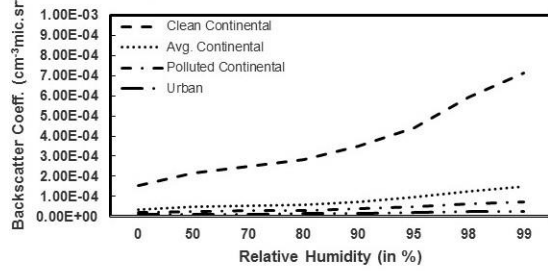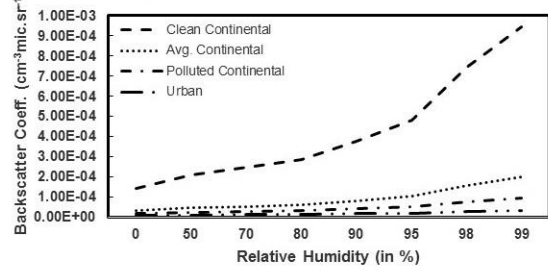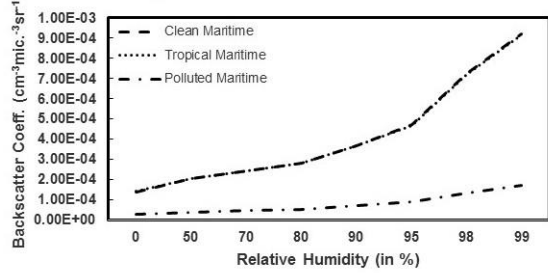
514

515   **Figure 3**: Variation in Backscattering Coefficient w.r.t. Relative Humidity for (a) Continental Aerosols and (b)
516   Maritime Aerosols at 532 nm and 1064 nm.

517
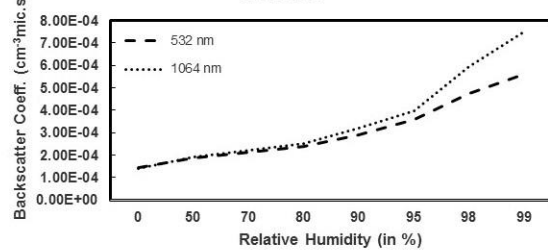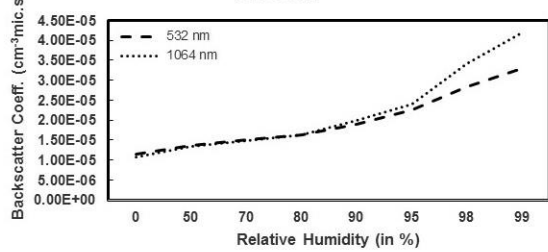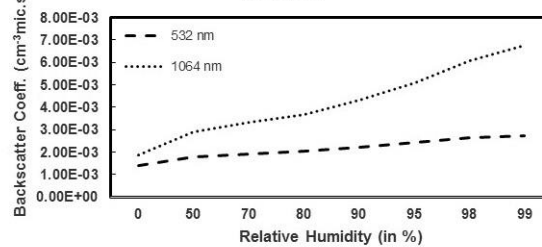
519

520   **Figure 4**: Variation in Backscattering Coefficient w.r.t. Relative Humidity for (a) Desert Aerosols and (b)
521   Arctic Aerosols and (c) Antarctic Aerosols at 532 nm and 1064 nm.

522

523

524

525
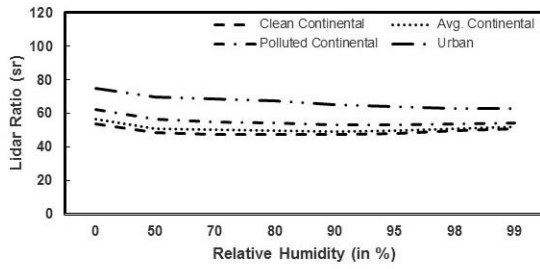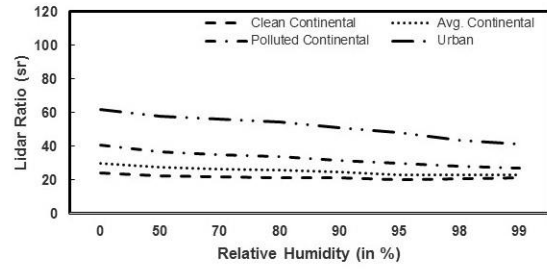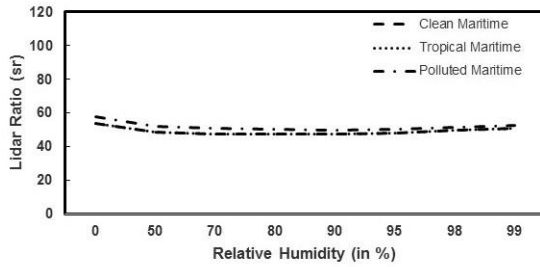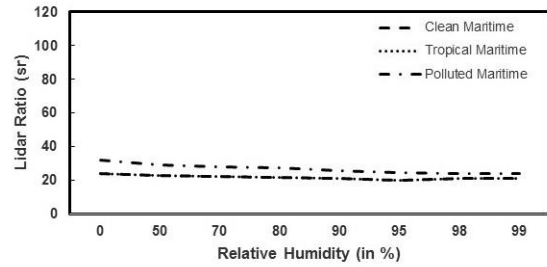
Figure 5: Variation in Lidar Ratio w.r.t. Relative Humidity for (a) Continental Aerosols and (b) Maritime
Aerosols at 532 nm and 1064 nm.

526
527
528

529

530
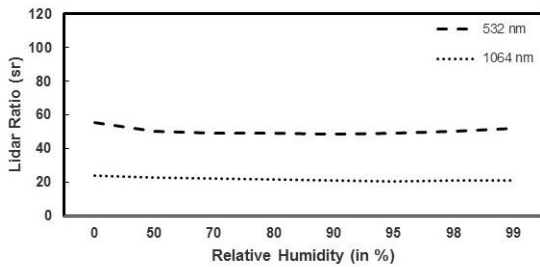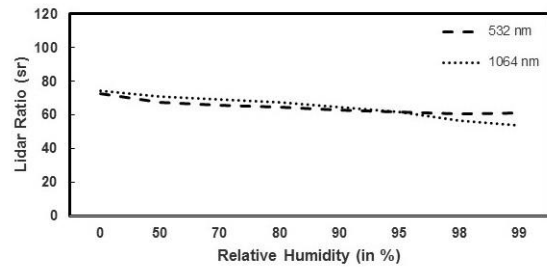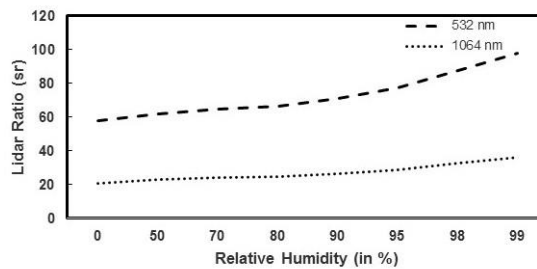
Figure 6: Variation in Lidar Ratio w.r.t. Relative Humidity for (a) Desert Aerosols and (b) Arctic Aerosols and
(c) Antarctic Aerosols at 532 nm and 1064 nm.

531
532
533
534
535

Table 1: Physical and Optical Properties of CALIPSO Aerosol Models (Omar et al. 2009)

Aerosol	$m_{r,532}$	$m_{i,532}$	$m_{r,1064}$	$m_{i,1064}$	$r_{m,fine}$ (μm)	σ_{fine}	$r_{m,coarse}$ (μm)	σ_{coarse}	μ_{fine}
Dust	1.414	0.0036	1.495	0.0043	0.1165	1.4813	2.8329	1.9078	0.223
Smoke	1.517	0.0234	1.541	0.0298	0.1436	1.5624	3.7260	2.1426	0.329
Clean Continental	1.380	0.0001	1.380	0.0001	0.20556	1.6100	2.6334	1.8987	0.050
Polluted Continental	1.404	0.0063	1.439	0.0073	0.1577	1.5257	3.5470	2.0650	0.531
Clean Marine	1.400	0.0050	1.400	0.0050	0.1500	1.6000	1.2160	1.6000	0.025
Polluted Dust	1.452	0.0109	1.512	0.0137	0.1265	1.5112	3.1617	1.9942	0.241

537

Table 2: Physical and Optical Properties of AERONET Aerosol Models at 673 nm classified using Cluster Analysis (Omar et al. 2005)

Aerosol	$m_{r,673}$	$m_{i,673}$	$r_{m,fine}$ (μm)	σ_{fine}	$r_{m,coarse}$ (μm)	σ_{coarse}	μ_{fine}
Category 1	1.4520	0.0036	0.117	1.482	2.834	1.908	0.22
Category 2	1.5202	0.0245	0.144	1.562	3.733	2.144	0.33
Category 3	1.4494	0.0092	0.133	1.502	3.590	2.104	0.38
Category 4	1.4098	0.0063	0.158	1.526	3.547	2.065	0.53
Category 5	1.3943	0.0044	0.165	1.611	3.268	1.995	0.26
Category 6	1.4104	0.0337	0.140	1.540	3.556	2.134	0.49

540

Table 3: Size Distribution of Aerosol Components for Models used in OPAC for Different Relative Humidities (d'Almeida et al. 1991 and Ackermann 1998)

Component	r_m (μm) (0%)	r_m (μm) (50%)	r_m (μm) (70%)	r_m (μm) (80%)	r_m (μm) (90%)	r_m (μm) (95%)	r_m (μm) (98%)	r_m (μm) (99%)	σ
Water Soluble	0.0212	0.0262	0.0285	0.0306	0.0348	0.0399	0.0476	0.0534	2.239
Insoluble	0.4710	0.4710	0.4710	0.4710	0.4710	0.4710	0.4710	0.4710	2.512
Soot	0.0118	0.0118	0.0118	0.0118	0.0118	0.0118	0.0118	0.0118	2.000
Mineral (nuc.)	0.0700	0.0700	0.0700	0.0700	0.0700	0.0700	0.0700	0.0700	1.950
Mineral (acc.)	0.3900	0.3900	0.3900	0.3900	0.3900	0.3900	0.3900	0.3900	2.000
Mineral (coa.)	1.9000	1.9000	1.9000	1.9000	1.9000	1.9000	1.9000	1.9000	2.150
Mineral (trans.)	0.5000	0.5000	0.5000	0.5000	0.5000	0.5000	0.5000	0.5000	2.200
Sea Salt (acc.)	0.2090	0.3360	0.3780	0.4160	0.4970	0.6050	0.8010	0.9950	2.030
Sea Salt (coa.)	1.7500	2.8200	3.1700	3.4900	4.1800	5.1100	6.8400	8.5900	2.030
Sulfate	0.0695	0.0983	0.1090	0.1180	0.1350	0.1580	0.1950	0.2310	2.030

543

Table 4: Refractive Indices of the Aerosol Components for the OPAC Aerosol Models used in this study (d'Almeida et al. 1991 and Ackermann 1998)

Component	$m_{r,532}$	$m_{i,532}$	$m_{r,1064}$	$m_{i,1064}$
Water Soluble	1.530	5.64×10^{-3}	1.520	1.64×10^{-2}
Insoluble	1.530	8.0×10^{-3}	1.510	8.00×10^{-3}
Soot	1.750	4.46×10^{-1}	1.760	4.43×10^{-1}
Mineral	1.530	6.33×10^{-3}	1.530	4.30×10^{-3}
Sea Salt	1.500	1.12×10^{-8}	1.470	1.95×10^{-4}
Sulfate	1.430	1.00×10^{-8}	1.423	1.50×10^{-6}
Water	1.333	1.61×10^{-9}	1.326	1.39×10^{-5}

546

547

Table 5: Composition of Aerosol Models used in OPAC (Hess et al. 1998)

Aerosol Types	Components	Number Mixing Ratio μ_i
Clean Continental	Water soluble	1.000
	Insoluble	0.577×10^{-4}
Average Continental	Water Soluble	0.458
	Insoluble	0.261×10^{-4}
	Soot	0.542
Polluted Continental	Water Soluble	0.314
	Insoluble	0.120×10^{-4}
	Soot	0.686
Urban	Water Soluble	0.177
	Insoluble	0.949×10^{-5}
	Soot	0.823
Clean Maritime	Water Soluble	0.987
	Sea Salt (acc.)	0.132×10^{-1}
	Sea Salt (coa.)	0.211×10^{-5}
Tropical Maritime	Water Soluble	0.983
	Sea Salt (acc.)	0.167×10^{-1}
	Sea Salt (coa.)	0.217×10^{-5}
Polluted Maritime	Water Soluble	0.422
	Sea Salt (acc.)	0.222×10^{-2}
	Sea Salt (coa.)	0.356×10^{-6}
	Soot	0.576
Desert	Water Soluble	0.870
	Mineral (nuc.)	0.117
	Mineral (acc.)	0.133×10^{-1}
	Mineral (coa.)	0.617×10^{-4}
Arctic	Water Soluble	0.197
	Insoluble	0.152×10^{-5}
	Sea Salt (acc.)	0.288×10^{-3}
	Soot	0.803
Antarctic	Sulfate	0.998
	Sea Salt (acc.)	0.109×10^{-2}
	Mineral (trans.)	0.123×10^{-3}

548

549

550

Table 6: Lidar Ratio (in sr) estimated using Mie theory for Omar et al. (2005) Aerosol Models

Aerosol Model	Desert Dust (Category-1)	Biomass Burning (Category -2)	Rural (Background) (Category-3)	Industrial Pollution (Category-4)	Polluted Marine (Category-5)	Dirty Pollution (Category- 6)
673 nm	28.68	46.92	36.27	44.20	45.18	48.87

552

Table 7: Lidar Ratio (in sr) Comparison between Theoretical values estimated using Mie Theory and In-situ values using Category-1 AERONET Data

Site/Year	2017	2018	2019	2020	2021	Mie Theory Estimate
Kanpur	53.67	47.32	50.31	54.12	50.46	28.68
Min.	36.06	21.31	30.76	32.03	29.41	
Max.	92.52	78.92	86.23	83.53	79.75	
	1998	**1999**	**2004**	**2005**	**2006**	
Bahrain	47.82	37.00	40.79	37.66	34.88	28.68
Min.	37.40	28.32	31.43	27.78	27.68	
Max.	69.67	81.69	53.60	64.40	45.83	
	2017	**2018**	**2019**	**2020**	**2021**	
Banizoumbou	49.96	52.04	50.98	49.88	51.12	28.68
Min.	27.80	29.08	37.20	32.10	41.83	
Max.	65.81	67.73	70.83	70.75	72.14	

555

Table 8: Lidar Ratio (in sr) Comparison between Theoretical values estimated using Mie Theory and In-situ values using Category-2 AERONET Data

Site/Year	2001	2002	2003	2004	2005	Mie Theory Estimate
Abracos Hill	52.95	53.89	51.87	50.52	55.30	46.92
Min.	44.99	41.63	32.30	44.24	39.87	
Max.	60.44	66.43	63.01	57.72	65.54	
	2016**	**2017**	**2018**	**2019**	**2020***	
Skukuza	38.47	49.37	43.01	44.04	63.24	46.92
Min.	19.14	32.50	34.98	28.56	63.24	
Max.	49.70	101.24	52.74	68.14	63.24	
	2014	**2015**	**2016**	**2017**	**2018**	
IMS Metu Erdemli	54.47	42.50	51.24	58.80	49.26	46.92
Min.	22.54	27.64	31.90	35.90	27.83	
Max.	69.72	61.70	73.60	75.06	67.43	

*Only single data value is available

**The data has an outlier. Without outlier the value of LR is 43.30 sr.

560

561

562

563

Table 9: Lidar Ratio (in sr) Comparison between Theoretical values estimated using Mie Theory and In-situ values using Category-3 AERONET Data

Site/Year	2002	2003	2005	2006	2009*	Mie Theory Estimate
Konza EDC	52.25	43.95	54.47	39.38	47.83	36.27
Min.	39.64	32.40	37.32	38.32	35.30	
Max.	64.46	73.75	85.26	40.45	58.52	
	2012	**2017**	**2018**	**2020**	**2021****	
Sevilleta	44.47	48.17	42.10	58.52	53.53	36.27
Min.	34.65	37.09	31.75	33.45	27.39	
Max.	56.64	57.99	56.59	78.83	72.29	
	2015	**2017**	**2018**	**2020**	**2021**	
Rimrock	46.45	49.98	47.41	47.43	47.65	36.27
Min.	37.53	35.03	29.97	39.36	33.47	
Max.	52.55	60.36	57.35	58.93	63.86	

*Only two data values are available

**The data has an outlier. Without outlier the value of LR is 50.40 sr.

Table 10: Lidar Ratio (in sr) Comparison between Theoretical values estimated using Mie Theory and In-situ values using Category-4 AERONET Data

Site/Year	2009	2012	2013	2014	2015	Mie Theory Estimate
Mexico City	54.44	56.86	56.99	64.40	63.40	44.20
Min.	23.16	37.61	39.66	47.48	36.68	
Max.	87.92	77.17	91.83	81.93	99.16	
	2003	**2004**	**2005**	**2006**	**2007**	
Moscow MSU MO	55.28	57.45	53.84	43.03	49.61	44.20
Min.	46.25	43.76	37.77	30.15	33.79	
Max.	68.83	71.03	77.44	55.44	68.28	
	2015	**2016**	**2017**	**2018**	**2019**	
GSFC	59.15	55.56	53.15	58.07	52.68	44.20
Min.	39.82	47.01	50.18	40.18	40.04	
Max.	67.93	60.78	55.15	68.84	61.79	

Table 11: Lidar Ratio (in sr) Comparison between Theoretical values estimated using Mie Theory and In-situ values using Category-5 AERONET Data

Site/Year	2002	2003	2011*	2012	2013	Mie Theory Estimate
Arica	62.45	69.22	67.68	73.63	62.94	45.18
Min.	44.66	52.14	67.68	69.62	41.86	
Max.	90.27	86.74	67.68	76.62	77.02	
	2004	**2005**	**2007**	**2008**	**2009**	
La Parguera	47.91	51.00	45.00	47.64	46.38	45.18
Min.	45.70	48.91	37.10	45.12	39.01	
Max.	50.72	56.92	51.73	50.99	52.49	
	2013	**2014**	**2015**	**2016**	**2017**	
Ascension Island	54.55	55.31	59.29	52.54	70.73	45.18
Min.	43.57	50.08	36.15	41.35	48.15	
Max.	67.64	62.07	74.13	67.57	92.67	

*Only single data value is available

Table 12: Lidar Ratio (in sr) Comparison between Theoretical values estimated using Mie Theory and In-situ values using Category-6 AERONET Data

Site/Year	2017	2018	2019	2020*	2021	Mie Theory Estimate
Dalanzadgad	52.80	41.68	47.58	37.85	47.43	48.87
Min.	39.46	32.05	41.55	37.85	38.27	
Max.	66.15	51.32	50.77	37.85	56.60	
	2016**	**2017**	**2018**	**2019**	**2020***	
Skukuza	38.47	49.37	43.01	44.04	63.24	48.87
Min.	19.14	32.50	34.98	28.56	63.24	
Max.	49.70	101.24	52.74	68.14	63.24	
	2014	**2015**	**2016**	**2017**	**2018**	
IMS Metu Erdemli	54.47	42.50	51.24	58.80	49.26	48.87
Min.	22.54	27.64	31.90	35.90	27.83	
Max.	69.72	61.70	73.60	75.06	67.43	

*Only single data value is available

**The data has an outlier. Without outlier the value of LR is 43.30 sr.

Table 13: Lidar Ratio (in sr) for Aerosol Models in CALIPSO Operational Algorithm

Wavelength/ Aerosol Model	Dust	Smoke (Biomass Burning)	Clean Continental	Polluted Continental	Clean Marine	Polluted Dust
Omar et al. (2009) CALIPSO V1 (based on in-situ measurements)						
532 nm	40	70	35	70	20	65
1064 nm	55	40	30	40	45	30
Lopes et al. (2013) CALIPSO LR Selection Algo. Evaluation (Mean ± S.D.)						
532 nm	40 ± 20	70 ± 28	35 ± 16	70 ± 25	20 ± 6	55 ± 22
Kim et al. (2018) CALIPSO V3 Operational Algo. (based on in-situ measurements)						
532 nm	40 ± 20	70 ± 25	35 ± 16	70 ± 25	20 ± 6	55 ± 22
1064 nm	55 ± 17	30 ± 14	30 ± 17	30 ± 14	45 ± 23	48 ± 24
Kim et al. (2018) CALIPSO V4 Operational Algo. (based on in-situ measurements)						
532 nm	44 ± 9	70 ± 25	53 ± 24	70 ± 25	23 ± 5	55 ± 22
1064 nm	44 ± 13	30 ± 14	30 ± 17	30 ± 14	23 ± 5	48 ± 24
Li et al. (2022) CALIPSO LR Selection Algo. Evaluation using SODA (Mean ± S.D.)						
532 nm (D)	42 ± 19	45 ± 17	-	45 ± 17	33 ± 15	52 ± 19
532 nm (N)	37 ± 13	57 ± 18	-	57 ± 18	33 ± 16	51 ± 18
In-house Derived in this study using Mie Theory						
532 nm	**38.72**	**63.37**	**85.98**	**64.73**	**57.31**	**48.22**
1064 nm	**20.11**	**33.68**	**31.98**	**26.44**	**71.11**	**25.56**